A model equation of state of liquid C_{60} and thermodynamic properties along the liquid–vapour coexistence curve

2005 J. Phys.: Condens. Matter 17 4411

(http://iopscience.iop.org/0953-8984/17/28/002)

INSTITUTE OF PHYSICS PUBLISHING JOURNAL OF PHYSICS: CONDENSED MATTER

J. Phys.: Condens. Matter **17** (2005) 4411–4422 doi:10.1088/0953-8984/17/28/002

A model equation of state of liquid C_{60} and thermodynamic properties along the liquid–vapour coexistence curve

M Bahaa Khedr[1,3], **M S Al-Busaidy**[2] **and S M Osman**[2,4]

[1] Physics Department, Faculty of Science, Banha University, Banha, Egypt
[2] Physics Department, College of Science, Sultan Qaboos University, PO Box 36, PC 123, Al_Kkod, Muscat, Sultanate of Oman

Received 29 November 2004, in final form 26 May 2005
Published 1 July 2005
Online at stacks.iop.org/JPhysCM/17/4411

Abstract

We present a model equation of state for C_{60} based on a variational series mean spherical approximation for a double Yukawa fluid. This allows us to investigate the liquid–vapour coexistence curve and calculate the thermodynamic properties of liquid C_{60}. The comparisons with computer simulation results, based on the Girifalco potential, suggest the importance of treating the attractive tail of the potential accurately. The estimated critical parameters, $T_c = 1943$ K, $\rho_c = 0.477$ nm^{-3} and $P_c = 34.2$ bar, are in good agreement with Gibbs ensemble Monte Carlo simulation predictions. The results are discussed, making reference to previous studies.

1. Introduction

Since the discovery by Krätschmer *et al* [1] of fullerene C_{60}, knowledge of the molecular and solid state chemistry of C_{60} has advanced rapidly. Many fullerene-derived solid phases have been synthesized with novel properties and potential applications [2]. The low temperature structure has been identified to be cubic $Pa3$ with orientationally ordered molecules [3]. At room temperature C_{60} molecules are known to undergo hindered rotations [4]. The high temperature data are sparse. The structure of liquid C_{60} is still of considerable interest [5]. Recently, inelastic neutron scattering spectroscopy experiments [6] have provided useful information on the complicated C_{60} structure and on the intermolecular interactions.

The structures of small $(C_{60})_N$ clusters, $2 \leqslant N \leqslant 25$ [7], and large clusters, $13 \leqslant N \leqslant 80$ [8], have been studied by means of molecular dynamics (MD) simulations. These calculations, based on the Girifalco [9] intermolecular potential, have predicted possible magic numbers in the size distribution of neutral $(C_{60})_N$ clusters. The large clusters lose the C_{60}

[3] Permanent Address: Faculty of Education, Bisha, PO Box 551, Kingdom of Saudi Arabia.
[4] Author to whom any correspondence should be addressed.

0953-8984/05/284411+12$30.00

molecular structure at temperatures of 700–800 K, which is in agreement with the experiment of Martin *et al* [10] at 800 K. The fullerenes slowly sublimated leaving graphitic carbon particles as a residue while recent MD simulations [11] have predicted that an isolated C_{60} molecule is stable against fragmentations up to ∼4500 K. In addition, the low density vapour phase is stable.

Hagen *et al* [12] reported a Monte Carlo (MC) simulation and concluded that C_{60} has no stable liquid phase, whereas the MD simulations of Cheng *et al* [13] and Rey *et al* [7] suggested that the liquid phase would only be observed in a narrower temperature range compared to that for rare gas systems. Hasegawa and Ohno [14] provided an explanation for the discrepancy between MC and MD simulations by showing the effect of the range of the attractive part of the pair potential on the free energy. The truncation of the pair potential, to save computer simulation time, leads to 5% reduction of the free energy which, in turn, leads to an ∼100 K shift of the liquid–vapour (L–V) phase boundary. Accordingly the liquid phase is suppressed towards the metastable phase, as appeared in the MC simulation of Hagen *et al* [12].

Quite recently, extensive Gibbs ensemble Monte Carlo (GEMC) simulations by Caccamo *et al* [15, 16] and constant-NVT Monte Carlo simulations by Hasegwa and Ohno [17, 18] were performed with the aim of establishing the effect of finite size on the existence of the L–V binodal line as well as on the location of its critical point. The GEMC simulations indicated that, with $N = 300$, 600 and 1600 particles, the overall shape of the binodal is not much influenced by finite size effects while both the critical temperature, T_c, and the critical density, ρ_c, have a tendency to become higher with increasing particle number N in the simulation box, which is in contradiction to the NVT MC results. It has also been reported [17] that the absolute free energy analysis used in the NVT MC simulations seems to suffer much less from the finite size effects.

The density functional theory (DFT) provides an accurate tool when it is combined with a thermodynamically consistent integral equation method. The DFT was applied to C_{60} in two advanced approximations, the simplified perturbation weighted density approximation (SPWDA) [19] and the generalized modified weighted density approximation (GMWDA) [14, 20]. Both approaches have predicted the existence of a liquid phase of C_{60} but in a very narrow range of temperature (<20 K) with $T_c = 1960$ K. The narrow range of the liquid phase has been ascribed [20] to the well known defect of the MWDA which is due to the shortcoming of the reference system as well as the hard sphere (HS) equation of state used.

On the other hand, highly accurate structural theories of fluids are applied to the determination of the phase diagram of C_{60}. The modified hypernetted-chain (MHNC) theory [21] agreed with the MD simulation on the existence of the liquid phase but over a wider range of temperature (1600 and 1920 K for the estimated triple point and critical temperature, respectively). The hierarchical reference theory (HRT) [22] yields rigorously flat isotherms which allows an accurate determination of the L–V coexistence curve without restoring the Maxwell equal area construction, which is known to have high uncertainty near the critical point. The HRT predicted a relatively high critical temperature $T_c = 2138$ K.

All previous computer simulations [7, 12–18] and theoretical calculations [14, 19–22] were based on the assumption of rigid spherical molecules interacting via a central potential. The well known Girifalco potential [9], $V_{Gr}(r)$, was used:

$$V_{GR}(r) = -\alpha\left[\frac{1}{S(S-1)^3} + \frac{1}{S(S+1)^3} - \frac{2}{S^4}\right] + \beta\left[\frac{1}{S(S-1)^9} + \frac{1}{S(S+1)^9} - \frac{2}{s^{10}}\right] \tag{1}$$

where $s = r/d$, $\alpha = \frac{N^2A}{12d^6}$ and $\beta = \frac{N^2B}{90d^{12}}$, with $N = 60$ atoms for C_{60} fullerene and d is its diameter. The parameters A and B belong to the 6–12 potential that describes the interaction

between two carbon atoms,

$$V_C(r) = -\frac{A}{r^6} + \frac{B}{r^{12}}. \tag{2}$$

According to Girifalco, the best values of A, B and d were obtained by fitting the experimental data for the heat of sublimation and the lattice constant of the FCC crystal. This procedure gives $d = 7.1$ Å, $A = 32.0 \times 10^{-60}$ erg cm^6 and $B = 55.77 \times 10^{-105}$ erg cm^{12}. Cheng *et al* [13] and Cheng and Klein [23] used $A = 23.8 \times 10^{-60}$ erg cm^6 and $B = 36.88 \times 10^{-105}$ erg cm^{12}. Very recently, Abramo *et al* [24] reported an atomistic molecular dynamics simulation in which the atomistic representation of a C_{60} molecule is taken into account, i.e. the spatial distribution of carbon atoms within the C_{60} fullerene is directly taken from experimental data, but still interacting via a 6–12 potential with the other set of adjustable parameters, A and B. These authors reported the superiority of the atomistic description of the potential over the early Girifalco central potential (Gr) in predicting experimental properties of C_{60} to an overall quantitative level of accuracy. Both atomistic simulations of Cheng *et al* [13] and Abramo *et al* [24] confirmed the existence of a dense fluid phase at temperatures above 1800 K. Also it has been reported that only at higher densities do the central potential and atomistic potential approaches yield rather different predictions for the energy and pressure and there are no substantial differences at low densities.

It is now well established from all above-mentioned computer simulations and integral equation approaches that the central pair interaction of rigid C_{60} molecules proposed by Girifalco [9] produces a stable liquid phase but in a narrow range of temperatures. This conclusion has also been confirmed by Alonso *et al* [25]. Of course C_{60} molecules have internal degrees of freedom. A modest acknowledgment of the assumption of non-rigidity is made in the study of Broughton *et al* [26]. They used a model potential of non-rigid C_{60} molecules in which the radius of each molecule, R_i, was allowed to be a dynamical variable, namely,

$$V_{Br}(r_{ij}) = \sum_{i<j} V(r_{ij}^-) + \sum_i J(R_i - R_0)^2, \tag{3}$$

where R_0 was set to be 3.571 Å and the so-called soft spring constant, J, was varied to give a breathing-mode frequency of 107.3 cm^{-1}. Broughton *et al* [26] acknowledged that this value of J is much lower than any of the experimentally observed intramolecular vibrational frequencies of C_{60}, which are in the 400–1600 cm^{-1} range. Broughton *et al* obtained the phase diagram of such a model of C_{60} by isothermal–isobaric molecular dynamics simulation (NPT MD). In their calculations no stable liquid phase was found. However, the model of non-rigid spheres proved to make some predictions of some properties of a metastable liquid phase, with critical thermodynamic constants $T_c = 1850$ K, $\rho_c = 0.51$ nm^{-3} and $P_c = 30$ bar. No doubt the non-rigidity of the molecules has an effect on the characteristics of the liquid phase, but one should be cautious with this model because of its limitation of using a quite low breathing-mode frequency.

A new intermolecular potential for C_{60} was derived from *ab initio* calculations by Pacheco and Prates [27]. The *ab initio* potential is considerably softer for short range forces than the Gr potential. Ferreire *et al* [28] used this new interaction potential in NVT MC simulations which predicted the existence of a liquid phase of C_{60} for densities between 0.845–0.468 nm^{-3} and temperatures between 1881 and 2012 K. These results are found to be much higher than all earlier simulations.

On the other hand, Guerin [29] reported a double Yukawa (DY) potential with parameters fitted with a Lennard-Jones potential in equation (2) for carbon–carbon interaction, with

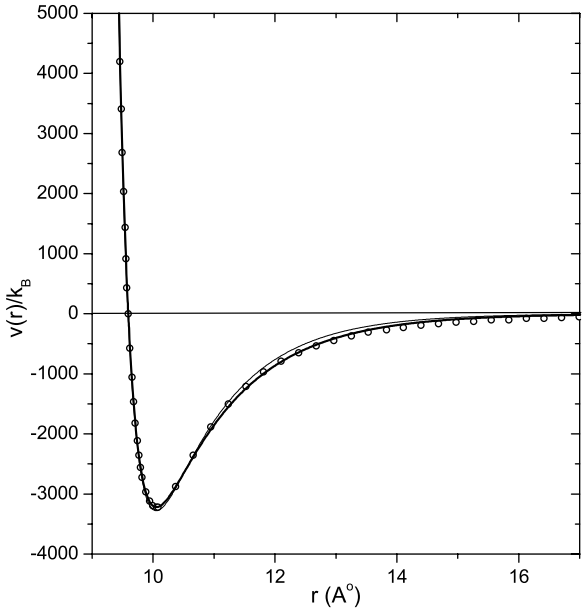

Figure 1. Intermolecular potential of C_{60}. The DY potential of the present work (solid thick line), the DY potential with parameters evaluated by Guerin [29] (solid thin line) and the Girifalco [9] potential (open circles).

parameters taken from [30]. Then integrating over C_{60} cages gave an effective pair potential for C_{60} molecules. $V_{DY}(r)$ is

$$V_{DY}(r) = \frac{E\varepsilon}{x}[e^{-\lambda_1(x-1)} - e^{-\lambda_2(x-1)}], \tag{4}$$

where $x = r/\sigma_0$, $\sigma_0 = 9.5904$ Å, $\varepsilon/k_B = 3277.7$ K, with k_B being Boltzmann's constant. $E = 1.8738$, $\lambda_1 = 40.736$ and $\lambda_2 = 7.4071$ are fitting parameters. ε and σ_0 are known to be the depth of the attractive well and the position of the zero of the potential, respectively.

In the present work we consider a system of rigid spherical C_{60} molecules interacting via a central potential. We employ the DY potential, equation (4), but with parameters fitted directly with the Gr potential, equation (1). Our fitting parameters are $\sigma_0 = 9.5929$ Å, $\varepsilon/k_B = 3218.5$ K, $E = 1.7293$, $\lambda_1 = 43.344$ and $\lambda_2 = 6.531$. A typical graph of the intermolecular potential for rigid C_{60} is shown in figure 1. The Guerin [29] DY potential has a slightly deeper well depth and shorter range of the attractive pocket comparable to both the Gr potential and our fitted DY potential. In section 2, we employ the variational scheme in calculating the L–V coexistence as well as the thermodynamic properties of the liquid phase. This is of particular interest since the analytical solution of the Yukawa closure is available in an accurate form within the series mean spherical approximation (SMSA) formalism, originally set up by Henderson [31] and reformulated and tested by Duh and Teràn [32]. In section 3, we present our results with comparison with available theoretical and simulation results. Finally, in section 4, a brief summary and conclusions of the work are given.

2. Theoretical formalism

We consider a system of N molecules of C_{60} interacting via a pair potential $V_{DY}(r)$ which can be split into a repulsive short range part $V_0(r)$ and a long range attractive part $V_1(r)$. Accordingly,

the Helmholtz free energy per particle of the system as a function of the number density, ρ, and temperature, T, can be written within the variational theory of classical fluids [33] as

$$\beta F \leqslant \beta F_0 + \beta F_1 \tag{5}$$

where $\beta = 1/k_B T$, F_0 is the free energy of the reference system and F_1 corresponds to the contribution from $V_1(r)$. As regards the choice of the reference system, we choose a suitable combination of scaled hard sphere (HS) entropy due to Bause and Colot [34] and the ideal gas contribution, namely,

$$\beta F_0 = -1 + \ln(\rho) - \frac{3}{2}\ln\left[\frac{2\pi m k_B T}{h^2}\right] + (a + 3b - 1)\ln(1-\eta) + \frac{(6 + 2a + 6b)\eta - (3 + 3a + 9b)\eta^2 + 2b\eta^3}{2(1-\eta)^2} \tag{6}$$

with $a = b = 2/3$ and $\eta = \frac{\pi}{6}\rho\sigma^3$ is the packing fraction. m denotes the molecular mass and h is Planck's constant. The scaling theory equation of state (EOS) for HS fluid is slightly more accurate than the well known Carnahan and Starling EOS [35]. The HS diameter σ depends on ρ and T via the Gibbs–Bogoliubov (GB) variational approach [33],

$$\left(\frac{\partial \beta F}{\partial \sigma}\right)_{\rho,T} = 0. \tag{7}$$

It may be noted that the optimizing diameter σ achieves a best free energy estimate of equation (5) and establishes the link between F_0 and F_1, where the latter stands for

$$\beta F_1 = 2\pi\rho \int_\sigma^\infty \beta V_1(r) g_{HS}(r) r^2 \, dr, \tag{8}$$

where $g_{HS}(r)$ is the HS radial distribution function. In equation (8), $V_1(r)$ can be replaced by $V_{DY}(r)$ from equation (4). The use of the DY potential further facilitates obtaining an analytical expression for F_1 by introducing the Laplace transform of $r g_{HS}(r)$, defined as

$$G(\lambda^*) = \int_1^\infty r^* g_{HS}(r^*) e^{-\lambda^* r^*} \, dr^*. \tag{9}$$

Equation (8) yields

$$\beta F_1 = \frac{12\eta E}{\sigma^* T^*}[e^{\lambda_1} G(\lambda_1^*) - e^{\lambda_2} G(\lambda_2^*)]. \tag{10}$$

In equations (9) and (10), we used the reduced quantities

$$\sigma^* = \frac{\sigma}{\sigma_0}, \qquad r^* = \frac{r}{\sigma}, \qquad \lambda^* = \lambda\sigma^*, \qquad \text{and} \qquad T^* = \frac{k_B T}{\varepsilon}.$$

One can readily derive the expressions for pressure, P, and chemical potential, μ, from equation (5) as

$$\beta P = \beta P_0 + \beta P_1 \tag{11}$$

and

$$\beta\mu = \beta\mu_0 + \beta\mu_1 \tag{12}$$

via the thermodynamic relations

$$\beta P = \rho^2 \left(\frac{\partial \beta F}{\partial \rho}\right)_T, \qquad \text{and} \qquad \beta\mu = \beta F + \frac{\beta P}{\rho}.$$

It is straightforward to obtain the derivatives of the free energy contributions F_0 and F_1 of equations (6) and (10), respectively, with respect to ρ, yielding

$$\beta P_0 = \frac{1+\eta+\eta^2-a\eta^3-b\eta^4}{(1-\eta)^3} \tag{13}$$

$$\frac{\beta P_1}{\rho} = \beta F_1 + \frac{12E\eta^2}{\sigma^* T^*}[\mathrm{e}^{\lambda_1} G'(\lambda_1^*) - \mathrm{e}^{\lambda_2} G'(\lambda_2^*)] \tag{14}$$

where

$$G'(\lambda^*) = \left(\frac{\partial G(\lambda^*)}{\partial \eta}\right)_T. \tag{15}$$

The detailed expression for $G(\lambda^*)$ can be obtained in an analytical form from the recently developed SMSA of [31, 32],

$$G(\lambda^*) = \frac{\mathrm{e}^{-\lambda^*}}{24\eta}\sum_{n=1}^{5}\frac{v_n(\lambda^*,\eta)}{nT^{*n-1}}. \tag{16}$$

The sub-functions $v_n(\lambda^*, \eta)$ are given explicitly in [32]. We took the analytical derivative of $G(\lambda^*)$ with respect to η but the final expression is too lengthy to accommodate in the present paper.

3. Results and discussion

To assess the quantity of the present EOS given in equation (11) we compare the pressure with the recent NVT MC simulation results of Hasegawa and Ohno [17]. Figure 2 illustrates typical examples of the pressure van der Waals loop as obtained from equation (11) and the NVT MC [17]. These results are generally in good agreement with the simulation results in the vapour and liquid branches of the van der Waals loop, whereas the middle section of the loop for the interfacial region does not show close fitting (but this will not have a dramatic effect on the overall phase boundaries). We note that the discrepancy between the pressure obtained from the low order virial EOS is $P = \rho k_B T[1 + B_2\rho + B_3\rho^2]$ with exact B_2 and B_3 [17] and the present EOS and the computer simulations results. This comparison indicates the superiority of the present EOS over the virial equation of state.

Next, we turn to the calculation of the L–V binodal line, following the thermodynamic conditions for phase equilibrium:

$$P(\rho_V, T) = P(\rho_L, T) \tag{17}$$

$$\mu(\rho_V, T) = \mu(\rho_L, T). \tag{18}$$

By enforcing equality of pressures and chemical potentials in the two phases at a fixed temperature we are able to determine uniquely the densities ρ_V and ρ_L of the coexisting vapour and liquid phases. This method fails in the vicinity of the critical temperatures where the van der Waals loop diminishes, yielding a large uncertainty in determining the critical parameters T_c and ρ_c. These parameters can be estimated by an analysis of the results in the vicinity of the critical point. Following a fitting procedure used by several authors [16–18], the L–V critical point was determined by assuming the scaling law $\rho_L - \rho_V = C(T_c - T)^{0.32}$ and the law of rectilinear diameters $\rho_L + \rho_V = 2\rho_c + D(T - T_c)$, where C and D are fitting parameters and 0.32 represents the critical exponent in the case of non-classical fluid. The values of T_c and ρ_c can be inserted in equation (11) to give the critical pressure P_c. The critical compressibility ratio can then be calculated, $Z_c = \frac{P_c}{\rho_c k_B T_c}$. The results for critical parameters for all previous calculations are reported for convenience in table 1. The pair potential used in each calculation is also shown

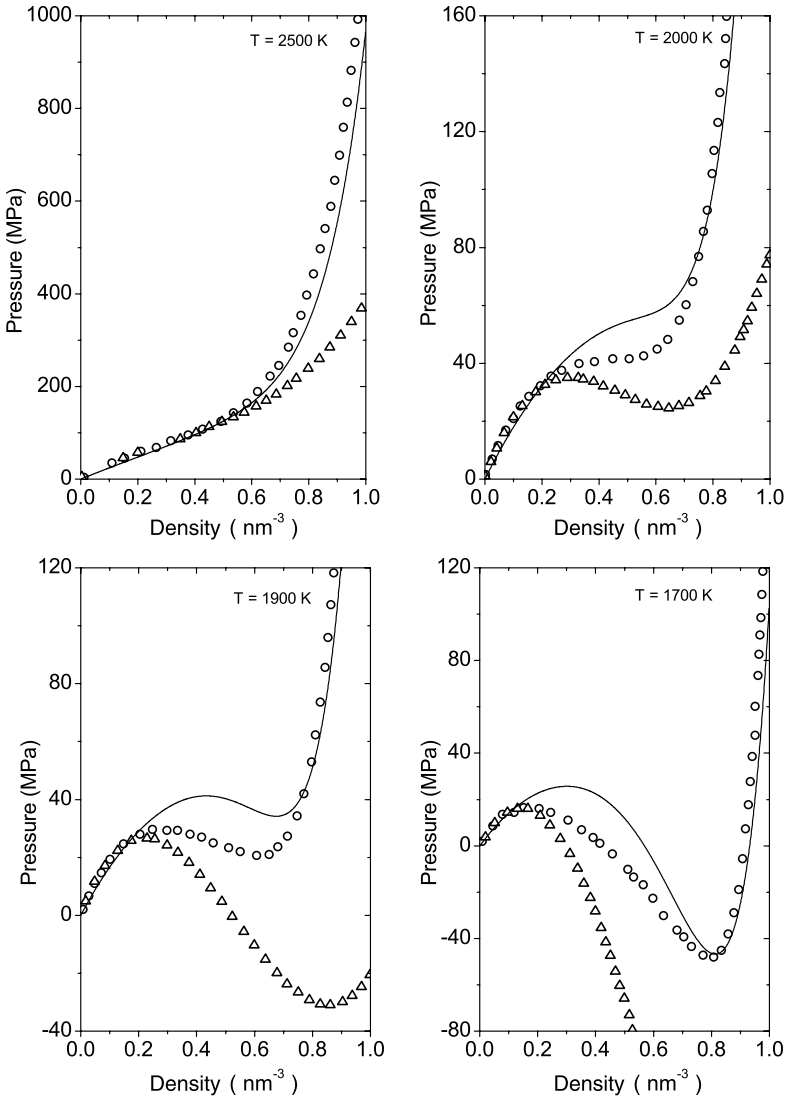

Figure 2. Comparison of the pressure from the present EOS obtained through equation (11) (solid line), the NVT MC simulation pressure [17] (open circles) and the virial pressure [19] (open triangles).

for better comparison. Our estimate of T_c agrees well with recent GEMC simulation results of Coccamo *et al* [15] while P_c and ρ_c are relatively overestimated. According to Alonso *et al* [25] Z_c should have a value near 0.29 for heavier condensed rare gases and 0.32 for C_{60} liquid–vapour transition. This prediction of Z_c is based only on the reported phase diagrams of Hasegawa and Ohno [17] and of Tau *et al* [22]. Surprisingly, the two approaches gave the same value of Z_c. Here we calculated Z_c for all reported phase diagrams and the results are presented in table 1. It is clear that this value of $Z_c = 0.32$, reported by Alonso *et al* [25], is not standard. According to our prediction as well as [15, 28], the value of Z_c may be around 0.28, which is even closer to the predicted value for the rare gas fluids and also agrees with the value of 0.27 that was calculated by March and Tosi [36] based on Dieterici's phenomenological

Table 1. Critical parameters of C_{60} compared with those of the previous theoretical calculations and computer simulations. The pair potential used in each calculation is shown as DY, GR and ab for double Yukawa, Girifalco and *ab initio* potential, respectively. In molecular dynamics (MD) and Monte Carlo (MC) computer simulations the number of particles N used in each simulation is indicated.

Method	Ref.	Pair potential	N	T_c (K)	ρ_c (nm^{-3})	P_c (bars)	Z_c
Present work		DY		1943	0.477	34.2	0.27
PY	[29]	DY		1940	0.5		
SPWDA	[19]	GR		2200	0.49		
GMWDA	[20]	GR		1960	0.41		
MHNC	[21]	GR		1920	0.43		
HRT	[22]	GR		2138	0.5	46.5	0.32
HMSA	[13]	GR		2050	0.56		
MD	[13]	GR	256	1900(100)	0.56(0.06)	25	0.17
GEMC	[12]	GR	256	1798(10)	0.42		
	[15]	GR	300	1924	0.39		
			600	1927	0.4	29	0.27
			1500	1941	0.42		
Free energy MC	[16]	GR		1940	0.42	27	0.24
NVT MC	[17]	GR	256	1980	0.439		
			500	1976	0.445	38	0.31
	[28]	ab	500	2011.7	0.4676	37	0.29
MD	[26]	Non-rigid spheres	256	1850	0.51	30	0.23

equation of state. It is important to mention that the low compressibility ratio of 0.23 for the non-rigid sphere model of Broughton *et al* [26] is due to the additional degree of freedom introduced by the low frequency isolated breathing mode, which leads to lower T_c, lower P_c and higher ρ_c than all other reported calculations.

Figures 3(a) and (b) show the high temperature phase diagram of C_{60} determined using the present EOS based on the variational series mean spherical approximation (VSMSA) formalism. In figure 3(a), the present results for the L–V binodal curve are compared with the GEMC results of Caccamo *et al* [15] obtained for $N = 600$ and 1500 and with NVT MC results of Hasegawa and Ohno [17]. Also we compare with similar calculations by Guerin [29] based on a similar DY potential but with the Percus–Yevick (PY) approximation for the hard sphere radial distribution function. We find that our results and both GEMC computer simulation results are in good agreement except in the critical region. In this comparison we note several points:

(i) Our predicted T_c of 1943 K agrees well with the GEMC result of 1941 K while our predictions of the critical density and pressure are ∼13% and ∼18%, respectively, higher than the GEMC predictions.

(ii) Both the present EOS and Guerin EOS [29] are based on the GB variational scheme. Our L–V coexisting densities show better agreement with the computer simulation than the Guerin results which indicates the improvement of the SMSA over the earlier PY approximation.

(iii) The results of the present theory overestimate the vapour density generally as well as in the vicinity of the critical point, which may be attributed to the shortcoming of either the GB variational scheme [33] at low density or the SMSA for the DY potential.

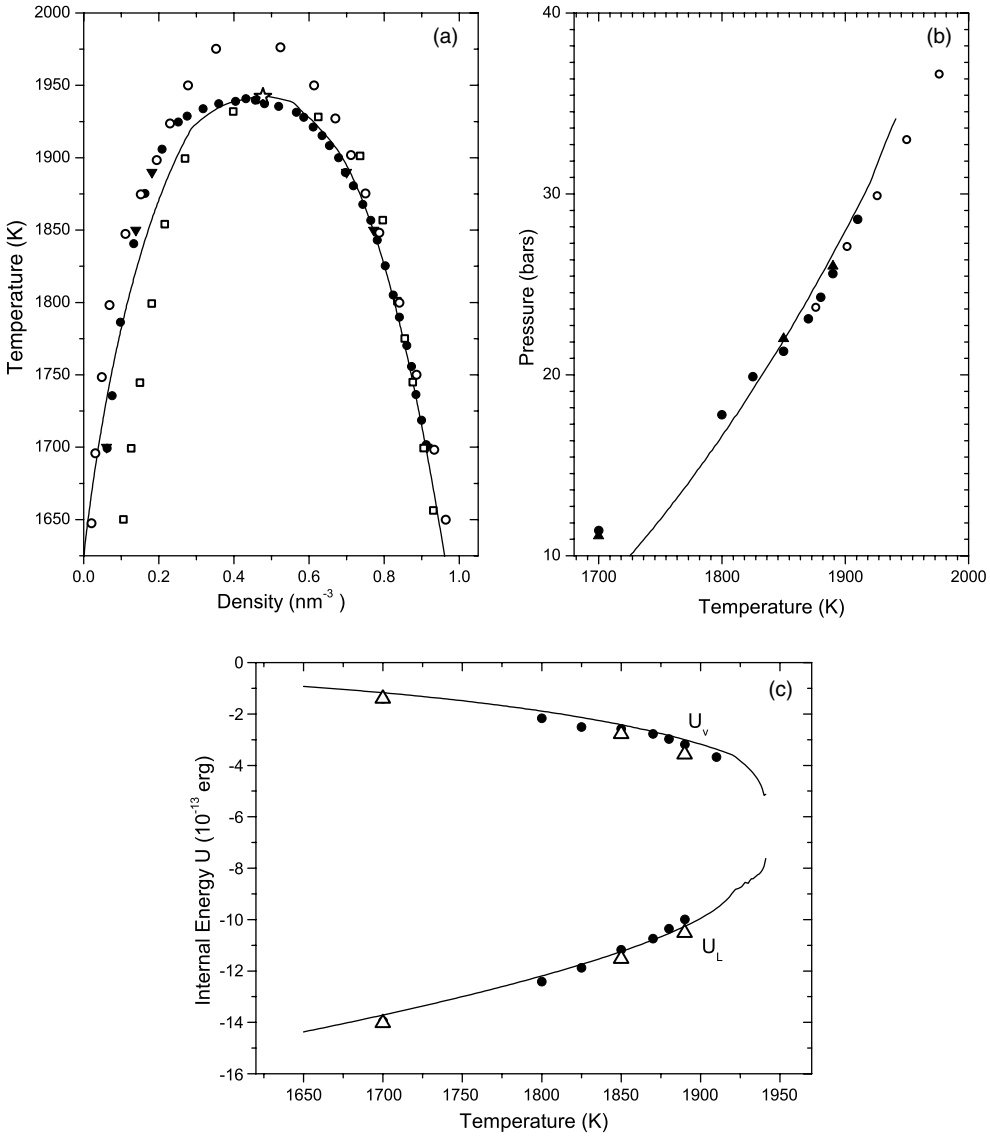

Figure 3. (a) Liquid–vapour coexistence curve of C_{60} obtained from the present model (solid line), the results of the GEMC of Caccamo *et al* [15] (solid circles for $N = 600$ and solid triangles for $N = 1500$), the NVT MC simulation results [17] (open circles) and the results of similar theoretical calculations by Guérin [29] (open squares). (b) Pressure versus temperature phase diagram corresponding to the binodal curve shown in (a): the present work (solid line), the GEMC simulations [15] ($N = 600$ solid circles, $N = 1500$, solid triangles) and the NVT MC simulations [17] (open circles). (c) Internal energy per particle of the coexisting liquid and vapour of C_{60}, U_L and U_V, respectively: the present work (solid line) and the GEMC simulations [15] ($N = 600$, solid circuits, $N = 1500$, open triangles).

Figure 3(b) shows the P–T representation of the phase diagram. It appears that the pressure calculated from the present model agrees well with the GEMC results [15] at intermediate temperatures and deviates substantially when approaching the critical temperatures. The accuracy of the treatment of the attractive force contribution via the SMSA can be assessed

Table 2. Thermodynamic properties of liquid C_{60} calculated along the liquid–vapour coexistence curve.

Temperature T (K)	Density P (nm^{-3})	Hard sphere diameter σ (Å)	Packing fraction η	Isothermal compressibility K_T (bar^{-1})	Entropy S (cal K^{-1})	Heat capacity C_v (cal mol^{-1} K^{-1})
1600	0.9755	9.5356	0.4429	0.271	35.712	3.024
1650	0.9446	9.5341	0.4286	0.353	36.332	3.085
1700	0.9105	9.5327	0.4130	0.480	36.971	3.148
1750	0.8719	9.5313	0.3953	0.694	37.644	3.216
1800	0.8269	9.5300	0.3747	1.106	38.368	3.290
1820	0.8062	9.5294	0.3653	1.393	38.682	3.322
1840	0.7833	9.5289	0.3549	1.824	39.016	3.358
1860	0.7572	9.5283	0.3430	2.539	39.380	3.397
1880	0.7270	9.5278	0.3292	3.858	39.784	3.441
1900	0.6883	9.5272	0.3117	7.207	40.275	3.494
1910	0.6627	9.5270	0.3000	11.864	40.584	3.529
1920	0.6280	9.5267	0.2843	28.512	40.988	3.573
1924	0.6146	9.5266	0.2782	42.288	41.142	3.588
1928	0.5981	9.5266	0.2708	77.736	41.328	3.606
1930	0.5903	9.5265	0.2672	106.836	41.416	3.614
1932	0.5817	9.5264	0.2633	160.644	41.512	3.623
1934	0.5737	9.5264	0.2597	233.630	41.601	3.630
1936	0.5668	9.5263	0.2566	290.170	41.678	3.636
1938	0.5584	9.5263	0.2528	383.090	41.772	3.643
1940	0.5344	9.5262	0.2419	3 022.299	42.030	3.664
1941	0.5185	9.5261	0.2347	6 247.065	42.199	3.676
1943	0.4771	9.5261	0.2159	12 568.68	42.640	3.700

by the internal energy comparison as the entropy effects are controlled largely by the hard sphere contribution. A more direct inspection of the accuracy of the SMSA at low and high densities is shown in figure 3(c). The internal energy per particle is compared with the GEMC simulations results along the bimodal curve. It is clear that U_L agrees well with the GEMC results while U_v deviates slightly. This explains the deficiency of the SMSA at low densities which is also obvious in figure 3(a).

Finally, we calculated the isothermal compressibility, $K_T = \frac{1}{\rho}(\frac{\partial \rho}{\partial P})_T$, entropy, $S = -(\frac{\partial F}{\partial T})_\rho$ and heat capacity at constant volume, $C_v = -T(\frac{\partial^2 F}{\partial T^2})_\rho$, using our model of C_{60} along the liquid side of the L–V coexistence curve. The results are given is table 2. It is worth mentioning that the hard sphere diameter σ shows the correct behaviour as it decreases with increasing temperature, which is expected for expanded liquids. The isothermal compressibility diverges rapidly on approaching the critical temperature, which is a typical criterion for the critical phenomena. Both entropy and specific heat change slightly along the L–V curve, which indicates that the smaller the entropic effect, the larger the energetic effect for enhancing the phase transition for materials with extremely short range attractive forces, as in the case of C_{60}. Unfortunately, there are neither experimental measurements nor computer simulation results available for comparison.

4. Summary and conclusions

The present equation of state is formulated from three main ingredients:

(i) the hard sphere reference system via the scaled particle theory for incorporating the contribution due to the short range forces among the C_{60} molecules;

(ii) the SMSA, which is employed via the double Yukawa potential to incorporate the effect of long range forces;
(iii) the suitable link between the free energy of the reference system and the contributions arising from the long range attractive interactions, established via the GB variational theory.

The present EOS is analytically derived with greater accuracy, which facilitates obtaining analytical expressions for the Helmholtz free energy and other thermodynamics functions. Moreover, the present EOS provides a ready-to-use model for C_{60}, which can be easily extended to other fullerenes of higher order such as C_{78}.

The L–V coexistence curve compares well with simulation results available in the literature for the Gr potential. The predicted critical parameters are consistent with the recent computer simulation results. However, the present theory shows two major deficiencies:

(a) the vapour density is overestimated, which, in turn, gives a higher critical density than that estimated by most computer simulations available;
(b) the predicted pressure is relatively high compared to other calculations, especially at high temperatures.

These deficiencies may be attributed to the shortcoming of the GB variational scheme [30] at low densities or the inaccuracy of the SMSA formalism at low densities. In order to clarify the uncertainties on this point, one needs to perform computer simulations on the double Yukawa system and compare with theoretical calculations, based on different perturbation schemes.

Acknowledgment

We are grateful to the Sultan Qaboos University for financial support. This work is part of the research project IG/Sci/Phys/03/04.

References

[1] Krätschmer W, Lamb L D, Fostiropoulos K and Huffman D R 1990 *Nature* **347** 354–8
[2] Zhou O and Cox D E 1992 *J. Phys. Chem. Solids* **53** 1373–90
[3] Heiney P A, Fischer J E, McGhie A R, Romanow W J, Denenstein A M, McCauley J P Jr, Smith A B and Cox D E 1991 *Phys. Rev. Lett.* **66** 2911–4
[4] Tycko R, Dabbagh G, Fleming R M, Haddon R C, Makhija A V and Zahurak S M 1991 *Phys. Rev. Lett.* **67** 1886–9
[5] Ashcroft N W 1991 *Europhys. Lett.* **16** 355
[6] Paci B, Deleuze M, Caciuffo R, Arduini A and Zerbetto F 2000 *Mol. Phys.* **98** 567–72
[7] Rey C, Gallego L J and Alonso J A 1994 *Phys. Rev.* B **49** 8491
[8] Doye J P K and Wales D J 1996 *Chem. Phys. Lett.* **262** 167–74
[9] Girifalco L A 1992 *J. Phys. Chem.* **96** 858
[10] Martin T P, Näher U, Schaber H and Zimmermann U 1993 *Phys. Rev. Lett.* **70** 3079
[11] Ohno K, Maroyama Y and Kawazoe Y 1996 *Phys. Rev.* B **52** 4078
[12] Hagen M H J, Meijer E J, Mooij G C A M, Frenkel D and Lekkerkerker H N W 1993 *Nature* **365** 425
Hagen M H J and Frenkel D 1994 *J. Chem. Phys.* **101** 4093–7
[13] Cheng A, Klein M L and Caccamo C 1993 *Phys. Rev. Lett.* **71** 1200–3
[14] Hasegawa M and Ohno K 1997 *J. Phys.: Condens. Matter* **9** 3361
[15] Caccamo C, Costa D and Fucile A 1997 *J. Chem. Phys.* **106** 255–63
[16] Costa D, Pellicane G, Abramo M C and Caccamo C 2003 *J. Chem. Phys.* **118** 304–10
[17] Hasegawa M and Ohno K 1999 *J. Chem. Phys.* **111** 5955–63
[18] Hasegawa M and Ohno K 2000 *J. Chem. Phys.* **113** 4315–9
[19] Mederos L and Nawascués G 1994 *Phys. Rev.* B **50** 1301

[20] Hasegawa M and Ohno K 1996 *Phys. Rev.* E **54** 3928
[21] Caccamo C 1995 *Phys. Rev.* E **51** 3387
[22] Tau M, Parola A, Pini D and Reatto L 1995 *Phys. Rev.* E **52** 2644
[23] Cheng A and Klein M L 1991 *J. Phys. Chem.* **95** 6750
[24] Abramo M C, Caccamo C, Costa D, Pellicane G and Ruberto R 2004 *Phys. Rev.* E **69** 31112
[25] Alonso J A, Lopez M J, March N H and Landan D 2002 *Phys. Chem. Liq.* **40** 457
[26] Broughton J Q, Lill J V and Johnson J K 1997 *Phys. Rev.* B **55** 2808
[27] Pacheco J M and Prates-Ramalho J P 1997 *Phys. Rev. Lett.* **79** 3873
[28] Ferreira A L C, Pacheco J M and Prates-Ramalho J P 2000 *J. Chem. Phys.* **113** 738–43
[29] Guerin H 1998 *J. Phys.: Condens. Matter* **10** L527
[30] Ali I, Osman S M, Al-Busaidi M and Singh R N 1999 *Int. J. Mod. Phys.* B **13** 3261
[31] Henderson D, Blum L and Noworyta J P 1995 *J. Chem. Phys.* **102** 4973
[32] Duh D-M and Mier-y-Teran L 1997 *Mol. Phys.* **90** 373
[33] Young W H 1992 *Rep. Prog. Phys.* **55** 1769
[34] Baus M and Colot J L 1987 *Phys. Rev.* A **36** 3912
[35] Carnahan N F and Starling K E 1969 *J. Chem. Phys.* **51** 635–6
[36] March N H and Tosi M P 1999 *Phys. Chem. Liq.* **37** 463